Available online at www.sciencedirect.com
SCIENCE DIRECT®
ELSEVIER
Journal of Magnetism and Magnetic Materials 293 (2005) 224–239
Journal of magnetism and magnetic materials
www.elsevier.com/locate/jmmm

Optical method for measurement of magnetophoretic mobility of individual magnetic microspheres in defined magnetic field

Urs O. Häfeli[a,*], Martin A. Lobedann[b], Julia Steingroewer[b], Lee R. Moore[c], Judy Riffle[d]

[a]*Faculty of Pharmaceutical Sciences, University of British Columbia, 2146 East Mall, Vancouver, BC, Canada V6T 1Z3*
[b]*Biomedical Engineering Department, 9500 Euclid Ave. T28, Cleveland, OH 44195, USA*
[c]*Institute of Food Technology and Bioprocess Engineering, Dresden University of Technology, Bergstrasse 120, 01069 Dresden, Germany*
[d]*Department of Chemistry, Virginia Polytechnic Institute, 2018 Hahn Hall, Blacksburg, VA 24061, USA*

Available online 2 March 2005

Abstract

The magnetophoretic mobility of magnetic microspheres, nanospheres and particles depends not only on type and amount of encapsulated magnetic compound, but also on microsphere-internal distribution, solvent system, porosity and other factors. Using a microscopic setup with automated digital image processing, different magnetic microspheres were investigated for size, acceleration and velocity of each single microsphere in the suspension. The overall magnetophoretic mobility (responsiveness to an external magnetic field) was not directly proportional to the saturation magnetization of the magnetic microspheres.

PACS: 07.55.−w; 07.55.Jg

Keywords: Velocity measurement; Magnetic microsphere; Microscopy; Imaging method; Magnetic susceptibility; Magnetophoresis; Magnetization; Characterization method

1. Introduction

Magnetic microspheres, nanospheres and particles (in the following summarily abbreviated as MMS) are promising drug delivery vehicles for clinical use. They have been applied to many diverse applications including tumor treatment by magnetic hyperthermia, the delivery of chemotherapeutic or radioactive drugs, the improved delivery of peptides for gene transfer, thrombolysis, detoxification of blood, delivery of antiinfective, antiarthritic, antifungal, and antiscar agents, and local anesthesia or neuroblockers [1]. MMS encapsulate a magnetic compound and can be made from

*Corresponding author. Tel.: +1 604 822 7133; fax: +1 604 822 3035.
E-mail address: uhafeli@interchange.ubc.ca (U.O. Häfeli).

0304-8853/$ - see front matter © 2005 Elsevier B.V. All rights reserved.
doi:10.1016/j.jmmm.2005.02.001

many different materials. Using the magnetic field of a permanent or electro-magnet, MMS can be guided inside a patient's body and magnetically concentrated in the region or organ of interest. The primary advantage of magnetic targeting, compared to current standard therapies, is that drug doses are significantly increased in the diseased target area and dramatically reduced in the surrounding healthy tissue, improving therapeutic efficacy and greatly reducing side effects [2].

In order to optimize the number of injected MMS that can be successfully guided to and trapped in the target area inside a person [3], the overall "magnetic responsiveness" of MMS must be known. Unfortunately, it is not sufficient to simply determine the magnetic susceptibility of MMS because this bulk property provides only a rough approximation of magnetic responsiveness for in vivo clinical situations. Other factors affecting magnetic responsiveness include the typically large size distribution of MMS, the physicochemical and surface properties of the many different matrix materials used to prepare MMS, and the amount, type and distribution of the magnetic compounds within the MMS [4]. The solvent system used and porosity, density, surface coating and aggregation tendencies of the MMS can further influence their overall magnetic responsiveness.

Because there are multiple factors that affect the magnetic responsiveness of MMS, direct methods for magnetic susceptibility measurements, such as a magnetic Faraday balance [5–7] or MRI techniques [8], have been replaced by more elaborate but indirect methods. One indirect system is field flow fractionation (FFF). In FFF, an external magnetic field is applied perpendicular to the flow direction [9,10], and the interaction of hydrodynamic and magnetic forces then separates the suspended MMS. The MMS retention ratio allows for the calculation of their magnetic susceptibility.

The analysis of MMS with FFF was made possible by the introduction of a 'cell tracking velocimetry' system. In this system, the movement of MMS or magnetically labeled cells in a well-defined magnetic field is videotaped [11]. The velocity of each particle passing the camera in laminar flow is then determined by tracking its movement. By comparing the data to MMS of calibrated magnetic susceptibility [12], information about their magnetic mobility and susceptibility is obtained. Magnetophoretic mobility is defined as $\mu_m = v_m/|\nabla B^2|$, where v_m is instantaneous velocity in a magnetic field B per unit driving force ∇B^2 [13,14].

The setup for cell tracking velocimetry is rather complicated, and our aim was to replace it with a simple stationary setup that can be used on a standard microscope equipped with a digital camera and computer system. Because our system takes into account all the factors which affect magnetic responsiveness, it functions as a test allowing the user to choose the most appropriate MMS for a specific clinical situation. It also allows for the analysis and comparison of the magnetophoretic mobility (i.e., the overall 'magnetic responsiveness' or amount of velocity for a given magnetic field and field gradient) of different types of MMS so that their behavior in a patient's circulation can be predicted. The main difference between this simplified system and the cell tracking system is that the geometry and size of the setup and magnets are considerably reduced.

2. Materials and methods

2.1. Principle of the magnetophoretic mobility determination in a stationary setup

If a single MMS submersed in a liquid medium is placed in the static magnetic field of a permanent of electro-magnet (Fig. 1), then a magnetic force $\vec{F}_m$, friction force $\vec{F}_S$, and gravitational force $\vec{F}_G$ act on it. The second law of mechanics can then be written as

$$\vec{F}_m + \vec{F}_S + \vec{F}_G = m\vec{a}, \quad (1)$$

where $\vec{a}$ is the acceleration and m is the mass of the particle. If the sum of these forces is larger than zero, the MMS will move toward the magnet, in the positive Y direction (see Fig. 1).

In order to describe the movement of the MMS in a static magnetic field H we assumed that (1)

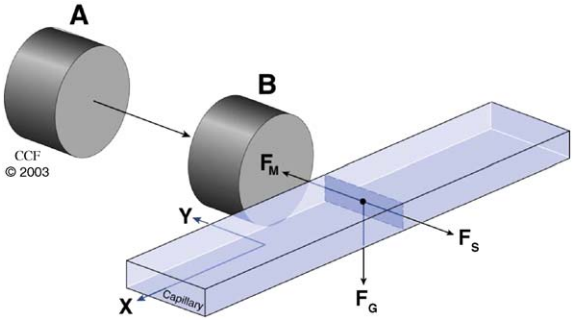

Fig. 1. Schematic drawing showing the forces acting on a magnetic microsphere inside a 2 mm wide and 0.1 mm high square capillary after moving the magnet from setup position A to measurement position B. The drawing is not to scale.

there is no interaction between MMS, (2) the MMS are perfect spheres, (3) the gravity force does not affect the movement of the analyzed MMS, (4) the product $H(\mathrm{d}H/\mathrm{d}y)$ is a constant, (5) the magnetic field in x-direction is constant ($\mathrm{d}H/\mathrm{d}x = 0$), and (6) the Reynold number of the MMS is less than 1 (i.e., the friction force becomes Stoke's force). Under these assumptions, we can neglect the gravity force and are left with the friction force

$$F_S = 6\pi\eta v r, \tag{2}$$

which depends on the radius r and velocity v of the particle, and the viscosity η of the solution. The magnetic force acting on a microsphere is

$$F_m = M\,\frac{\mathrm{d}H}{\mathrm{d}y}, \tag{3}$$

where

$$M = \chi\mu_0 H V_{MMS} f_m, \tag{4}$$

where χ is the volumetric permeability of the MMS, μ_0 is the permeability of free space, V_{MMS} is the volume of the MMS and f_m is the constant volume fraction of the magnetic component. The magnetic force then becomes

$$F_m = H\,\frac{\mathrm{d}H}{\mathrm{d}y}\chi V_{MMS} f_m. \tag{5}$$

To estimate the velocity of the MMS, the forces can be set to equal

$$F_S = F_m \tag{6}$$

as was demonstrated by Senyei et al. [15]. Solving for the velocity gives

$$v = \frac{V_{MMS}\chi\mu_0 H(\mathrm{d}H/\mathrm{d}y)}{3\pi\eta D}, \tag{7}$$

where D is the diameter of the MMS.

When analyzing MMS of the same type with identical shape and homogeneous distribution of the magnetic component, but different particle diameter, the velocity can be expressed as a function of the changing radius r or diameter D as

$$v = \frac{2r^2 f_m\chi\mu_0 H(\mathrm{d}H/\mathrm{d}y)}{9\eta} = \frac{D^2 f_m\chi\mu_0 H(\mathrm{d}H/\mathrm{d}y)}{18\eta}. \tag{8}$$

Doubling the size of a MMS, with all other properties the same, will thus increase the velocity by a factor of 4.

Velocity measurements can be tricky to make because of the varying physical properties of MMS, especially their density and size. For this reason, the medium viscosity must occasionally be adjusted. The viscosities were analyzed using a Brookfield Digital Viscosimeter (Brookfield Engineering Laboratories, Stoughton, MA). The velocity v_{Viss} in a higher viscosity solution can be converted into a velocity in water v_{H_2O} for comparison purposes using the equation

$$v_{H_2O} = v_{Vis}\frac{\eta_{Vis}}{\eta_{H_2O}}\left(\frac{D_{H_2O}}{D_{Vis}}\right)^2. \tag{9}$$

2.2. Properties of the static magnetic field

The magnetic field across the square capillary in Fig. 1 was measured with a transversal gauss probe Sypris Test & Measurement model 6010 (Sypris Solutions, Inc, Louisville, KY), starting in the centerline of the magnet, from its surface to 20 mm away from the surface. The step size was 0.1 mm, and the probe was mounted on and moved with a syringe pump (Harvard Apparatus, model PHD 2000 Programmable 70-2002, Holliston, MA). The magnetic field is shown in Fig. 2.

The magnetic field in the centerline at a distance of 40–50 mm away from the surface was also characterized. When the capillary is filled with new

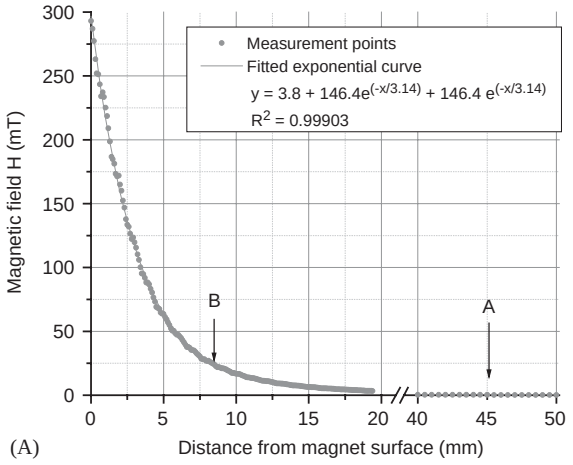

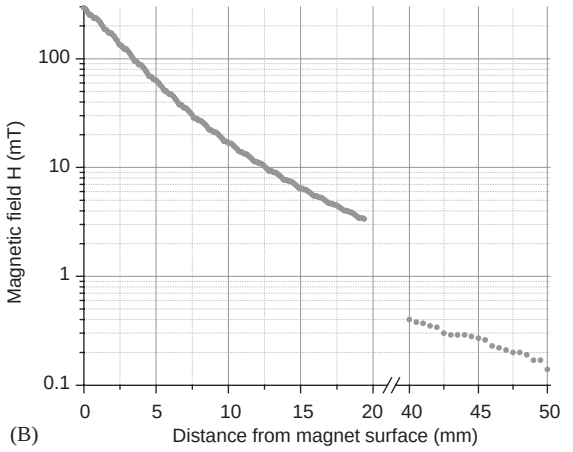

Fig. 2. Characterization of the magnetic field in (A) normal and (B) logarithmic form from a 10 mm diameter and 3 mm thick NdFeB magnet of 35 MGO in both measurement (B at 8.5 mm) and parking (A at 45 mm) position.

MMS, the magnet surface rests in a defined position 45 mm away from the capillary. As observed in the microscope, the magnetic field of below 0.3 mT at that position was unable to move the MMS and was thus used as the magnet "parking" position.

Optimally we would like the product of the magnetic field B and field gradient $\mathrm{d}H/\mathrm{d}y$ in the measurement area to be a constant since this implies that the velocity of magnetically attracted MMS is constant (see Eqs. (6) and (7)). Due to the

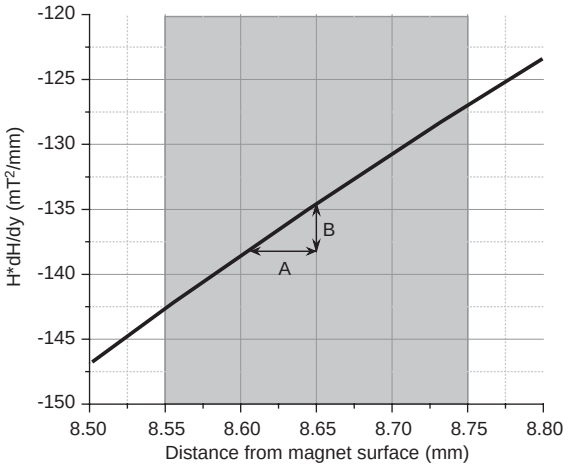

Fig. 3. Change of the product $H(\mathrm{d}H/\mathrm{d}y)$ in the area observed in the microscope. (A) Represents the typical distance of one track, which a MMS travels in one measurement. (B) Represents the product change within this track.

fact that we only used a simple NdFeB disk magnet (Dexter Corp., Chicago, IL) it is not possible to keep this product constant. However, the magnetic force can be seen to be constant within a typical track of 25 μm since the change in the magnetic field strength is only 1.5%, and can thus be neglected. Within the area observed in the microscope (gray area in Fig. 3) at a distance of 8.55–8.75 mm from the magnet, the product $H(\mathrm{d}H/\mathrm{d}y)$ changes about 16 $(\mathrm{mT})^2/\mathrm{mm}$.

2.3. Experimental setup

To image the MMS, the inverse microscope Leica DM IRB (Chatsworth, CA) with a Photometrics Cool Snap HQ camera (Tucson, AZ) at a resolution of 1392×1040 pixels and $1.6\times$ zoom adapter were used (Fig. 4a). A pixel size of 0.2 μm was achieved by using a $20\times$ objective. A piece of acrylic ($9 \times 19\,\mathrm{cm}^2$) was taped on a custom-made, lower than usual (6 mm), microscope table. This made it possible to lay the capillary lower, so that the center of the magnet and the capillary were level with the focus plane. A flat capillary with an inner diameter of 0.1×2 mm (Vitrocom Inc., Mountain Lakes, NJ) was placed in the acrylic piece and filled with a well-mixed microsphere

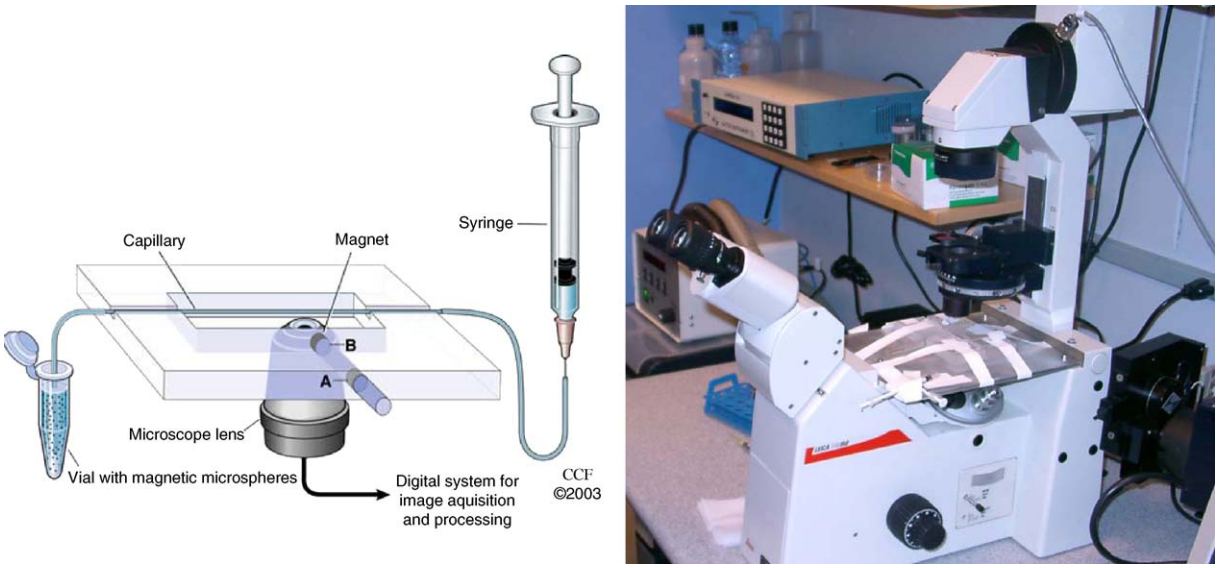

Fig. 4. (A) Schematic and (B) actual setup of the microscopy table and inverted microscope for measurements.

suspension using a 1 ml syringe (Fig. 4a). In contrast to earlier first tests with a round capillary [16], a flat capillary was used this time, thus preventing optical distortions and allowing more exact MMS size measurements. The MMS concentration used depended on the particle size (the smaller the particles, the lower the concentrations) and was found to be ideal between 0.01 and 0.05 mg/ml.

During the filling of the capillary, the magnet was 45 mm away from the capillary in position A (Fig. 4a). The microscope was manually focused so that a clear picture was displayed on the screen of the windows-based PC. The MMS stopped moving in the X direction (Fig. 1) within 5–10 s and the magnet was then manually moved into position B, 8.65 mm away from the center of the capillary. The magnetic field in this measurement position was ~22.5 mT and the field gradient at the center of the capillary ~6 mT/mm. The repeatability of setup was within $\pm 60\,\mu m$.

Using stream acquisition, 92 frames were automatically recorded using the software MetaMorph 6.0 (Universal Imaging Corporation^{TM}, Downingtown, PA), a program normally used for the live imaging of cell movements. With stream acquisition the data stream is directly saved to RAM before being written to a hard drive. The resulting stack of 92 successive frames with $2^{12} = 4096$ gray levels was analyzed with MetaMorph. A threshold was set manually for the MMS appearing as dark spots on a bright background, the MMS of interest marked and their diameters measured automatically. Fig. 5 shows a screenshot of MetaMorph. Of interest for our analysis were only the MMS which did not hit other MMS, were not agglomerated, and did not get stuck on the glass surface of the capillary. All diameter values were written to an Excel file using DDE (dynamic data exchange). MetaMorph was then used to follow the marked particles in a fully automated fashion through the entire stack of 92 frames and to compute the tracks through the entire sequential file. The analysis included measuring the x,y-position of each individual MMS in the first frame and in each successive frame and then calculating the velocity of the track. The dataset was again sent to the Excel file for storage and further analysis.

The MMS always moved in the positive y direction through the frames, but small movements in the x direction were also observed. This movement was caused not by the magnet, but by small solvent currents in the capillary. Since the x movement was very small and did not affect the

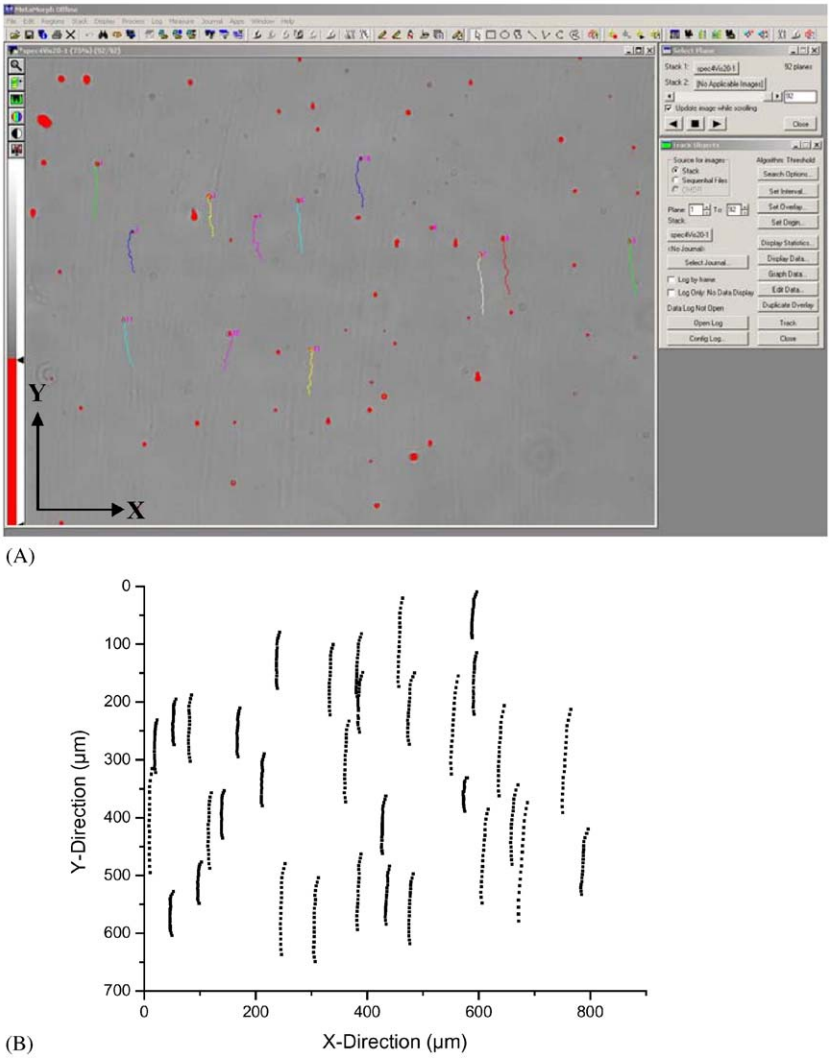

Fig. 5. (A) Interface of the software MetaMorph showing 12 analyzed tracks of Specimen 4 in 20% sucrose solution. MMS above a certain threshold show up red. The magnet is placed on top. (B) Depiction of the MMS tracks (here with Dynabeads) after data analysis and removal of the non-analyzed particles.

movement in y direction, we only used the y movements for the velocity calculations.

2.4. MMS used for analysis

Several types of MMS were used to test our method, spanning the spectrum from particles used in laboratory assays and cell extraction to those used in clinical magnetic targeting (Table 1). Up to 80 MMS were analyzed at once. To analyze higher numbers of MMS, another stream acquisition was performed after suspending the MMS anew in the capillary by simple syringe mixing.

2.5. Cell tracking velocimetry as a verification method

Cell tracking velocimetry (CTV) is a method to measure cell magnetophoresis. We applied it here to two MMS samples and compared the results to

Table 1
Properties of the tested MMS and results of the measurements in our setup

Specimen	Comments	Density (g/cm^3)	Saturation magnetization (emu/g)	Magnetization per MMS (emu/MMS)	Nominal size (μm)	Measured mean diameter ± SD (μm)	Test solvent	Mean velocity ± SD (μm/s)	Number of analyzed MMS
Specimen 1-SiMAG/H-2 T *	Maghemite core (orange)	2.25	28.22	3.19×10^{-11}	1.77 ± 0.61	1.72 ± 0.38	Water	4.11 ± 1.47	110
Specimen 2-SiMAG/H-T/55 *	Maghemite core	2.25	44.56	3.82×10^{-12}	0.48 ± 0.65	1.00 ± 0.32	Water	1.12 ± 1.50	50
Specimen 4-SiMAG-K/10 *	Magnetite core (black)	2.25	26.64	5.46×10^{-11}	1.75 ± 0.58	1.74 ± 0.41	Water	4.30 ± 1.67	141
Specimen 4 *	Magnetite core (black)	2.25	26.64	5.46×10^{-11}	1.75 ± 0.58	1.53 ± 0.38	Sucrose 20%	1.67 ± 0.72	149
Specimen 4 *	Magnetite core (black)	2.25	26.64	5.46×10^{-11}	1.75 ± 0.58	1.49 ± 0.38	Sucrose 40%	1.01 ± 0.39	462
Specimen 4 *	Magnetite core (black)	2.25	26.64	5.46×10^{-11}	1.75 ± 0.58	1.65 ± 0.47	Sucrose 60%	0.16 ± 0.10	343
Specimen 6-SiMAG/K-TCL/V *	Magnetite core	2.25	16.10	2.88×10^{-11}	1.43 ± 0.69	1.52 ± 0.39	Water	2.64 ± 1.03	160
Specimen 7-SiMAG-10 *	Maghemite core	2.25	32.28	6.31×10^{-11}	1.17 ± 0.56	1.66 ± 0.46	Water	3.07 ± 1.70	221
Specimen 9-SiMAG-50 *	Maghemite core	2.25	24.50	4.29×10^{-11}	0.57 ± 0.54	1.43 ± 0.39	Water	1.73 ± 0.66	231
Dynabeads M280 [1]	Polystyrene microspheres with 12% γ-Fe_2O_3	1.30	8.77	1.61×10^{-12}	2.80 ± 0.20	2.70 ± 0.42	Water	12.50 ± 3.99	242
PLA-MMS 10% [2]	Poly(lactic acid) microspheres with 10% Fe_3O_4	1.30	7.64	9.82×10^{-12}	—	1.89 ± 0.63	Water	1.15 ± 1.90	90
Magnetite coated [3]	Magnetite coated with itaconic acid	5.18	83.86	3.75×10^{-10}	—	1.65 ± 0.41	Sucrose 40%	1.64 ± 0.94	192
Magnetite uncoated [3]	Uncoated magnetite	5.18	79.72	3.55×10^{-10}	—	1.64 ± 0.40	Sucrose 40%	1.61 ± 1.06	89
MTC KB [4]	Iron-carbon particles with 88% iron	4.10	132.01	—	mostly 1-2	2.76 ± 1.10	Sucrose 60%	2.51 ± 2.09	61
Glass MMS [5]	Magnetite < 15 w% (about 1/3 of it part of the glass matrix)	4.60	3.68	3.19×10^{-11}	< 20	3.60 ± 1.99	Sucrose 40%	3.82 ± 3.74	36
Sicastar-M [6]	Silica	2.50	9.69	4.28×10^{-11}	1.50 ± 0.37	2.21 ± 0.57	Water	7.65 ± 2.94	150

The nominal size was determined by laser diffraction measurements, the measured mean diameter is the one determined on the analyzed MMS sample by optical microscopy. Producers: *Chemicell, Berlin, Germany; [1]Dynal, Norway; [2]Hafeli et al. [21]; [3]Riffle, Blacksburg, VA; [4]FeRx Inc., San Diego, CA; [5]MO-SCI Corp., Rolla, MO; [6]Micromod, Rostock, Germany.

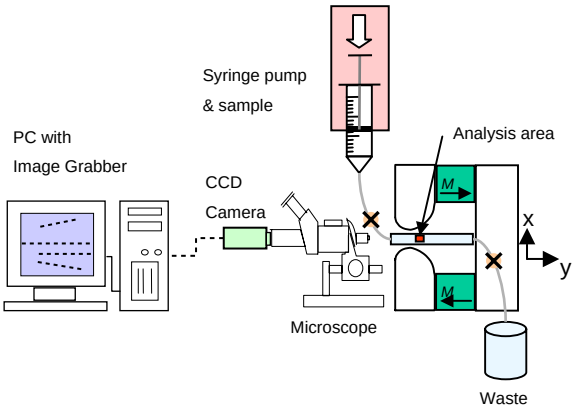

Fig. 6. Setup of the CTV system.

the method under investigation. The principles and practice of CTV have been thoroughly discussed elsewhere [12,17,18]. The central part of the apparatus (Fig. 6) is a permanent magnet assembly, with specially designed pole pieces that produce a nearly constant value for the product of field and field gradient: $H(\mathrm{d}H/\mathrm{d}y) = 1.115 \pm 0.008 \times 10^{14}\,\mathrm{A^2/m^3}$. Spaced 2.5 mm apart, the pole pieces conduct the magnetic flux into an air gap, into which a 0.6 mm × 1.7 mm ID, 0.4 mm wall rectangular channel is placed. The orientation of the magnet and flow channel ensures that the field is essentially two-dimensional, allowing us to neglect the z component. The major component of the magnetic force is orthogonal to gravity, in order to avoid the sedimentation contribution to the magnetophoretic velocity. To compute velocities, only the horizontal component of the gradient is thus used.

In the viewing area, the field strength H was $1.033 \pm 0.066 \times 10^6\,\mathrm{A/m}$ (mean ± 1 SD), and the field strength gradient was $1.082 \pm 0.087 \times 10^8\,\mathrm{A/m^2}$. After a volume of MMS suspension was pumped into the channel, the flow was stopped and valves on either side of the channel closed to ensure motionless fluid. The MMS motion in the quiescent fluid was observed with a 5× microscope objective and 2.5× photo eyepiece (Olympus, Tokyo, Japan), which gave a viewing area of 1.72 × 1.27 mm (width × height) and a nominal depth of field of 20 μm. A Cohu (San Diego, CA) CCD 4915 camera operating at a frame speed of 30 Hz, and a μ-Tech Vision 1000 PCI Bus Frame Grabber (MuTech Corp., Billerica, MA) were used to convert the image into a 640 × 480 pixel array, where each pixel contained eight bits of gray-level information ranging from 0 (black) to 255 (white). The internal code used five successive images to establish the most probable path for a specific MMS. From this most probable path, the algorithm determined and reported the 2-D location. A linear fit of the location-time data gave the magnetic migration velocity of each particle, v_m. The algorithm then computed statistics for the entire set of particle velocities, including mean, standard deviation and confidence limits. A wide range of particle velocities was measured by varying the acquisition rate, with the highest rate (each frame is acquired) used for the fast MMS, and a lower rate (every nth frame is acquired, $n = 2,\ldots,$ 100 or higher) used for the very slow particles.

The expected magnetic drift velocities were calculated with the aid of Eq. (7). It was assumed that the particle susceptibility was much larger in magnitude than that of the suspending medium, so that $\chi - \chi_\mathrm{m}$ in the general equation (7) becomes just χ. As a practical matter, we evaluated the susceptibility of the entire volume of the particle without differentiation of its constituents: magnetite/maghemite and polymer matrix. So r became the radius of the particle, not its magnetite core, and f_m became 1. The particle susceptibility was evaluated from $\chi = M(H)/H$, where induced volumetric magnetization M depends on the field strength, which itself depends on position. Magnetometer measurements of specimens 1 and 4 showed that at the field strength of the CTV magnet, these particles were well into saturation. So $M(H)$ became a constant M_satt, the saturation magnetization. The susceptibility became $\chi = M_\mathrm{sat}/\langle H\rangle$, where $\langle H\rangle$ was the average value in the viewing area. The volumetric saturation magnetization in SI units was found from the dipole moment μ_satt given in emu units and measured by the magnetometer as

$$M_\mathrm{sat}[\mathrm{SI}] = 1000\,\frac{\mu_\mathrm{sat}}{m}\,\rho, \tag{10}$$

where m is the sample mass in g, ρ is sample density in g/cm^3, and 1000 is a unit conversion factor.

3. Results and discussion

Our inverted microscope-based system for the measurement of magnetophoretic mobility was easy to use and produced repeatable results. A complete measurement took about 15 min, with the sample preparation taking about 5 min, the measurement 10 s, and the semi-automated analysis about 10 min. Table 1 lists the overall results of different MMS measurements.

The correlation between the measured magnetophoretic mobility of the MMS in water and their saturation magnetization was unexpected. We expected MMS with a higher bulk magnetization to have higher magnetophoretic mobility, but this was not the case for our measurements (Fig. 7). Hence it was clear that factors other than saturation magnetization control the behavior of MMS under the influence of a magnetic field. One possible factor could be that our measurements were performed in a magnetic field that was less than 10% of the magnetic field required for saturation. Testing was done under such conditions to simulate in vivo magnetic targeting. The

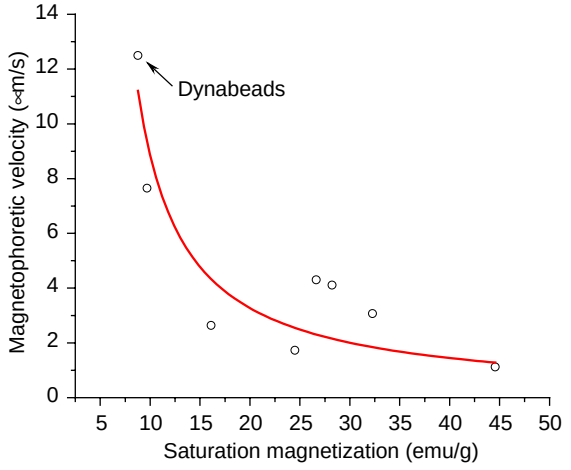

Fig. 7. Correlation between measured magnetophoretic mobility of the MMS in water and their saturation magnetization.

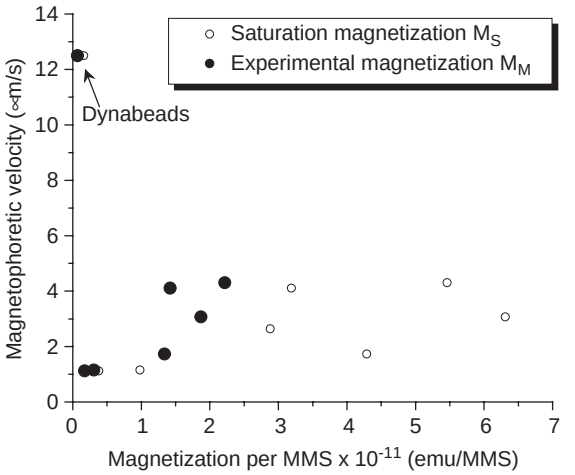

Fig. 8. Magnetization per MMS using the saturation magnetization M_S for each MMS and the experimentally used measurement magnetization M_M.

low magnetic field results not only in a lower magnetization, but also in distinctly different slopes of the magnetization curve of different MMS. Fig. 8 shows the average magnetization of MMS for both the magnetically saturated and the experimental conditions. Under experimental magnetization conditions the magnetophoretic velocity approximates the expected behavior, with the exception of Dynabeads. Dynabeads reached a plateau in magnetophoretic velocity despite the magnetization being only 43% of the saturation magnetization value. This might have to do with the fact that Dynabeads are truly superparamagnetic and have the steepest magnetization curve of all MMS tested here (not shown).

Another factor that may have contributed to our unexpected magnetophoretic velocity results is that the speed of the MMS were not constant during the measurements due to changing magnetic field and gradient. An analysis of many single MMS from different MMS types, however, showed that this was not a contributing factor. MMS velocity on average was actually relatively steady over the 10 s measurement time. The assumption that the product of magnetic field and its gradient are constant in our measurement setup thus appears to be correct. Fig. 9 shows the velocity of 3 individual MMS over time. The

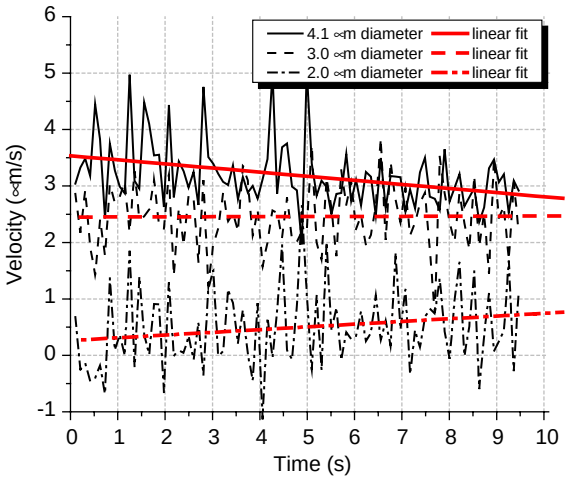

Fig. 9. Velocity change of three individual glass MMS in 40% sucrose solution during the 10 s analysis.

velocity does not change more than $\pm 20\%$ of the mean velocity of one MMS. These variations in velocity are not caused by the increasing magnetic field, since there is on average no upward trend, but are most likely due to the method of image capturing used. Due to the relatively slow movement of magnetic particles and the high frame rate, the MMS only move a few pixels per frame. The movement of one pixel more or one pixel less thus leads to a relatively large difference (in percent), producing the strong fluctuations in velocity around the mean velocity.

Another factor that could have influenced our measured magnetophoretic velocity is gravity. Our measurement system is not able to take the effect of gravity into consideration since the MMS are observed from the top and thus any vertical movement cannot be measured. Once a MMS sinks to the bottom of the capillary and stops moving, it disappears from the analysis and does not falsify the result. In water as a media, this happens to MMS with a diameter larger than 6 μm and a density higher than 4 g/cm^3. We dealt with this problem by adjusting the viscosity of the media when high density MMS were used (see full discussion of viscosity effects four paragraphs down). If the MMS sink to the bottom of the glass capillary and are then dragged along towards the magnet, the observed velocity would be diminished by a (difficult to determine) kinetic friction factor μ_K. The interaction between glass bottom and MMS are not currently known and may be very different for MMS made from different matrix materials.

An important factor for the correct determination of the magnetophoretic velocity is the size distribution of the analyzed MMS. As expected from Eq. (8), the MMS velocity increases with increasing diameter. This can be nicely seen in the magnetophoretic mobility data in water of three magnetic silica microsphere types with different size distributions (Figs. 10A–C) or uniformly sized larger MMS (Fig. 10D). Analyzing a batch of magnetic glass microspheres with a wider size distribution shows this effect even more clearly (Fig. 11). The data can be approximated with a quadratic function. Deviations from the calculated line might be due to the inconsistent ratio of magnetic to non-magnetic material between MMS, and the limitations in accurately sizing the MMS with our setup.

The ability to analyze every single MMS for its magnetophoretic velocity is a unique, and we believe, central feature of our measurement method. In order to deliver highly potent, and thus often also highly toxic drugs to a target location with the help of MMS, it is important to be able to predict the behavior of all, and not just the average, MMS in a batch. In this way, appropriate magnets can be designed and correct magnetic field strengths applied for the optimal delivery of specific MMS at a defined depth in the body of a patient. Knowing the particle's overall behavior also allows to determine what type of MMS would be best for the application and then rationally design MMS with these properties. For example, MMS might have to be made larger, with a uniform size distribution, or with a higher content of the magnetic component. Any potential agglomeration effects will also become evident during the measurements. Agglomerations in the small blood vessels can lead to embolization in vivo and must be avoided by for example choosing a smaller MMS size.

The measurements in our setup are limited by the microscope resolution and magnification. The

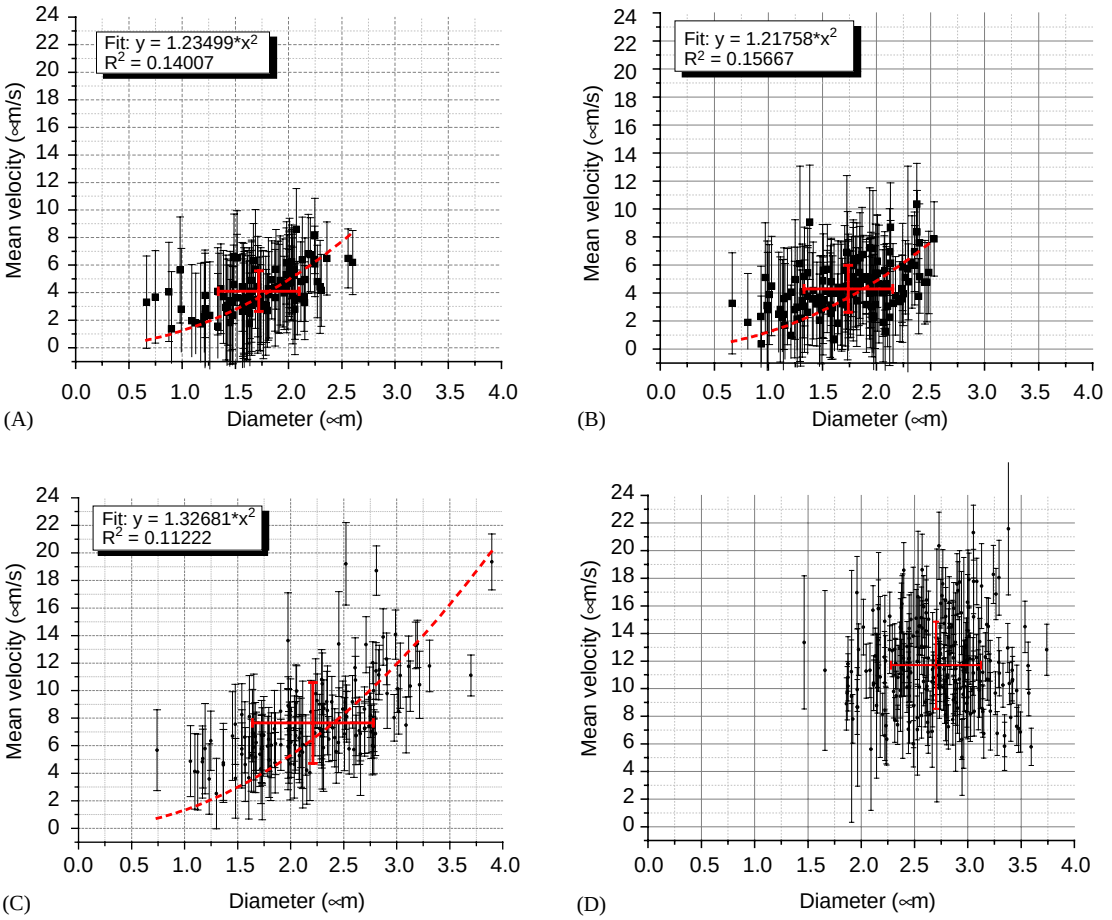

Fig. 10. Measured velocities of different MMS. (A) Specimen 1, (B) Specimen 4, (C) Sicastar-M, and (D) Dynabeads M280. Each point represents the mean speed of one track ± 1 SD.

smallest traceable MMS diameter is about 0.4 μm. An increase in magnification to 40× or 100× would be possible, but our current setup does not allow for this because the objective would interfere with the flow chamber. True magnetic nanospheres can thus not be analyzed. In addition, at these higher resolutions the Brownian motion becomes evident with the smaller MMS. They often move rapidly out of focus and are thus not pursuable, leading to an overrepresentation of the larger particles. These effects, however, only become important at MMS sizes below 0.8 μm.

Most of the measurements were done in water. To delay sedimentation in MMS with high densities, solvents with a higher viscosity are often used. This is also true in a clinical setting where MMS are often injected in viscous sugar solutions to prevent settling out. Using Specimen 4 we performed a few measurements with higher viscous solutions. With increasing viscosity, the porous silica MMS slowed down as expected (Fig. 12). Applying Eq. (9), the equivalent velocities in water were then calculated (Table 2). At lower viscosities the calculated velocities agreed well with the velocity measured in water. At viscosities above 5 cP, however, the deviations increased rapidly and reached more than 100% (Table 2). Since the reasons for these deviations are unknown, it might

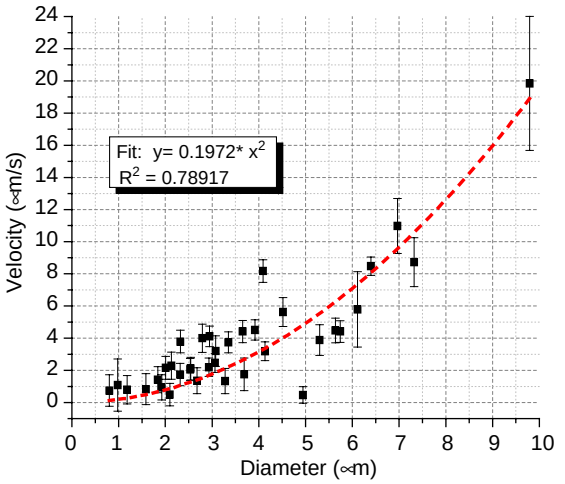

Fig. 11. Glass MMS with a wider size distribution show the quadratic relationship between particle size and MMS velocity.

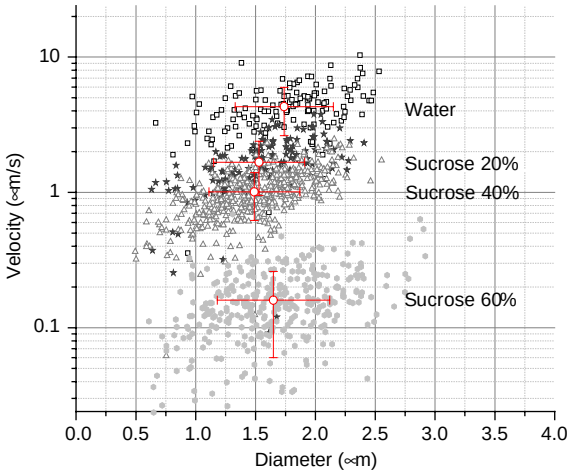

Fig. 12. Influence of the viscosity of the suspension media on magnetophoretic mobility, as measured with Specimen 4 MMS in sucrose solutions.

be advantageous to perform the measurements for the time being in solutions with lower viscosity.

3.1. Comparison of our results to theoretical calculations

The most direct way of checking our results is by calculating an expected magnetophoretic mobility using Eq. (9). This was done for all analyzed MMS, using the measured size distributions, the viscosities tabulated in Weast [19], the magnetization at the measurement position as interpolated from the magnetization curves of each MMS batch, and the magnetic energy density gradient $(H \times \mathrm{d}H)$ of $8.55 \pm 0.28 \times 10^{10}\,\mathrm{A^2/m^3}$. In this group of 12 rather different MMS (Table 3), the Dynabeads were the only MMS which fit the calculated data almost exactly (−2.5%). All other measured velocities were much lower than calculated, i.e., an average of $78.0 \pm 20.8\%$ lower.

To investigate the possibility that our method introduced such large errors, we performed an error propagation analysis. For the error analysis, it is important to understand the magnetic make-up of the MMS. The MMS are composed of a magnetic component (magnetite, maghemite or iron) and often a non-magnetic component (typically, a polymer). The magnetometer measures the gross magnetization of the particles, and does not distinguish between the contributions of the components. Using this macroscopic perspective, the susceptibility is found from the gross magnetization, the particle diameter is that of the entire particle, and f_{m} becomes unity. The theoretical expression of the particle magnetophoretic velocity is then given by Eq. (8). The uncertainties due to random error, in each of the variables D, χ, η and

Table 2
Converted velocity in water after measurement of Specimen 4 MMS in higher viscous solutions

Solvent	Viscosity (cP) ± 1 SD[a]	Converted velocity in water (μm/s)	Mean difference (%)
Water	0.933 ± 0.060	4.30[b]	0.0
Sucrose 20%	1.94 ± 0.10	4.32	0.5
Sucrose 40%	6.16 ± 0.80	9.09	111.4
Sucrose 60%	58 ± 16	11.56	169.0

[a] At 23 °C, as given by Weast [19].
[b] Measured.

Table 3
Comparison of calculated and measured velocities. Uncertainties are given at one standard deviation

Sample[a]	Diameter (μm)	Viscosity (cP)	Calculated velocity (μm/s)	Measured velocity (μm/s)	Measured velocity, 95% CI (μm/s)	Difference (%)
Specimen 1	1.72±0.38	0.933±0.060	28.3±9.2	4.1±1.5	(3.84, 4.38)	−85.5
Specimen 2	1.00±0.32	0.933±0.060	16.2±7.5	1.1±1.5	(0.70, 1.54)	−93.1
Specimen 4	1.74±0.41	0.933±0.060	29±10	4.3±1.7	(4.02, 4.58)	−85.3
Specimen 6	1.52±0.39	0.933±0.060	106±40	2.6±1.0	(2.48, 2.80)	−97.5
Specimen 7	1.66±0.46	0.933±0.060	21.2±8.5	3.1±1.7	(2.85, 3.29)	−85.8
Specimen 9	1.43±0.39	0.933±0.060	12.6±5.0	1.73±0.66	(1.64, 1.82)	−86.3
Dynabeads M280	2.70±0.42	0.933±0.060	12.8±3.1	12.5±4.0	(12.0, 13.0)	−2.5
PLA-MMS 10%	1.89±0.63	0.933±0.060	4.0±1.9	1.2±1.9	(0.76, 1.54)	−71.0
Magnetite coated	1.65±0.41	6.16±0.80	28±11	1.64±0.94	(1.51, 1.77)	−94.2
Magnetite uncoated	1.64±0.40	6.16±0.80	29±11	1.6±1.1	(1.39, 1.83)	−94.4
MTC KB	2.76±1.10	58±16	5.1±3.2	2.5±2.1	(1.99, 3.03)	−50.3
Glass MMS	3.60±1.99	6.16±0.80	5.5±4.3	3.8±3.7	(2.60, 5.04)	−30.0
Sicastar-M	2.21±0.57	0.933±0.060	20.2±7.6	7.6±2.9	(7.18, 8.12)	−62.2

[a]See Table 1.

$H(\mathrm{d}H/\mathrm{d}y)$ contribute to the expected dispersion in velocity. The permeability of free space, μ_0, is a precisely known constant equal to $4\pi \times 10^{-7}$ and f_m is set to 1.0, so these contribute nothing to the dispersion.

Given an equation $F = axyz$, where F is calculated from constant a and independent variables x, y and z, the uncertainty in F, $\Delta(F)$ is

$$\Delta(F) = F\sqrt{\frac{\Delta^2(x)}{x^2} + \frac{\Delta^2(y)}{y^2} + \frac{\Delta^2(z)}{z^2}}, \tag{11}$$

where $\Delta^2(x)$, $\Delta^2(y)$ and $\Delta^2(z)$, are the squares of uncertainties (variances) of each of the independent variables.

The particle magnetic susceptibility is calculated from:

$$\chi[\mathrm{SI}] = 1000\frac{\mu(\langle H\rangle)\rho}{m\langle H\rangle}. \tag{12}$$

From the magnetization curve obtained from the magnetometer, we found the value of the dipole moment μ, in emu units, at the mean field strength of the magnetophoretic system $\langle H\rangle$. The mass of particles sampled in the measurement is m, and ρ is the particle density. In this treatment, m and ρ are in CGS units and $\langle H\rangle$ is in SI units. Sample mass measurements and magnetic field measurements have typically a 2% uncertainty each, and we therefore ascribe an uncertainty of 5% to the susceptibility calculation.

The uncertainty of the product $H \times \mathrm{gradH}$ is estimated from that of a uniform distribution where a particle has equal probability of being observed over a 0.2 mm interval: $\sigma = (f(x2) - f(x1))/(12)^{0.5}$. So, $f(x1)$ and $f(x2)$ correspond to the value of $H \times \mathrm{gradH}$ at the limits. Inserting these values gives the standard deviation listed in Table 3. The uncertainty in viscosity was estimated by allowing for the effect of a 5 °C temperature range on the tabulated viscosity of water. For solutions with sucrose the temperature effect is small compared to that of uncertainty in solution preparation when a window of 5% is allowed. The relative error is larger at higher sucrose concentration, as seen by comparing the measurements of sample 4 (Table 2), due to the exponential rise of viscosity with concentration for most solutes. Eqs. (8) and (9) were applied to give the mean and standard deviation in expected velocity u. Since the diameter is squared in Eq. (8), the uncertainty must be counted twice, and this variable is thus the

major contributor to uncertainty in velocity. The relative error in velocity is about one third or higher.

The fifth column of Table 3 lists the mean ± 1 SD of the measured particle magnetophoretic velocity. The relative error in the measured velocity is comparable to that of the calculated velocity. But the means of measured velocities are consistently lower—much lower—than expected. This suggests a systematic rather than random cause. The 95% confidence interval of the measured mean velocity is fairly narrow, due probably to the large sample size. The measured confidence interval and the interval defined by calculated mean velocity ± 1 or even 2 SD rarely overlap.

Although we expected differences between the calculated and measured magnetophoretic velocities (after all, that was the reason for starting this investigation), it is not clear why there is such a large systematic discrepancy between the two. Even more interesting is the fact that the uniform Dynabeads which are homogeneously filled with superparamagnetic magnetite/maghemite behaved almost exactly as calculated. Is it possible that the size of the MMS and the distribution of the magnetic component have such huge effects on MMS behavior in magnetic fields which do not produce magnetization saturation?

There are indications in the literature that the intraparticular distribution of the magnetic component, in particular, is very important, sometimes even more important than the mass (bulk) magnetization of the magnetic component. Duguay wrote in 1991 in his master's thesis [20] that using 10% iron instead of nickel encapsulated into poly(lactic acid) MMS increased the retention rate in tubing with an attached magnet by over 23% (Table 4). Similarly, using magnetite instead of nickel also significantly increased the retention rate by almost 24%. Although the differences between the retention rate of nickel and the other two magnetic materials can be simply explained by the differences in mass magnetization, the lack of difference between iron and magnetite cannot be explained by this approach. Duguay considers the distribution of the magnetic component and describes in an appendix that a 3-fold difference in necessary magnetic forces is possible when comparing a relatively homogenously distributed magnetic compound such as magnetite to the more peripherally embedded iron carbonyl globules in the MMS. In addition, Duguay mentions that magnetite of the encapsulated size is inherently ferromagnetic, and considerable interaction can thus take place between the MMS. Overall, the change in magnetic material might thus be less important for retention (or magnetophoretic behavior) than changing the physical form and MMS internal distribution.

3.2. Comparison of our results to CTV measurements

Another way of checking our experimental results is to compare them to the well-established Cell Tracking Velocimetry method. The measurement chamber of the CTV instrument looks similar to our own, but is arranged vertically rather than horizontally (Fig. 4) and uses a much stronger permanent magnet. The magnet produced a magnetic field H of 1.3 T and a gradient of the magnetic field dH/dy of 0.14 T/mm. We performed

Table 4
Retention of poly(lactic acid) MMS encapsulating 10% of three different magnetic compounds in a flow system, as described by Duguay [20]

Magnetic component	Size of magnetic component (μm)	Retention rate of MMS with 10% magnetic component	Magnetic component distribution	Mass magnetization (emu/g)
Nickel	$<\sim 0.8$	X	Relatively homogeneous	54.4
Iron carbonyl	6–8	$X+23\%$	Peripheral around MMS	218
Magnetite	0.47	$X+24\%$	Relatively homogeneous	90

The microspheres had an average size of 50–70 μm.

Table 5
Comparison of CTV-determined velocities with calculated velocities for two MMS samples

	M_{sat} (A/m)	χ (SI)	Diameter (μm)	Calculated velocity (μm/s)	CTV velocity; mean ± SD (μm/s)	Difference (%)	Particles analyzed
Specimen 1	32,339	0.03131	1.72	67.47	48.9 ± 30.2	−27.6	2730
Specimen 4	27,531	0.02665	1.74	58.78	65.8 ± 27.0	11.9	820

CTV measurements in a 60% glycerol solution with a viscosity of 10.68 cP [19], since particles with high magnetite content tend to have high velocities and need to be slowed down for optimal imaging. For the comparison, we chose two MMS samples, specimens 1 and 4, measured their magnetophoretic mobility, and compared them to the values calculated with the help of Eq. (8). The resulting velocities in Table 5 are closer to the calculated values than our microscopic measurements, although the deviations were still 27% and 11% for specimens 1 and 4, respectively. Considering that these were the first measurements and efforts of tracking such highly magnetic particles by CTV, the listed differences between calculated and measured velocities seem acceptable. The rather large standard deviation of the measured velocities, i.e., ±30%, is likely caused by intrinsic variation in magnetite loading and diameter between individual particles, variation in H and thus variation in χ across the tracking region, and indeterminate instrument noise. Note that because of the large number of tracked particles, the confidence interval of the mean velocity is quite small. CTV does not assign the size of each MMS measurements and the results are thus always averages. The microscopic method on the other hand directly suggests the optimal size distribution.

In conclusion, our method is straightforward and gives a distribution of MMS sizes and their related magnetophoretic velocities. Our method, however, does not appear to measure true magnetophoretic velocities as defined by Moore et al. [12]. We confirmed this by comparing the results to calculated magnetophoretic velocities, measured bulk mass magnetizations, and cell tracking velocimetry measurements. An extensive error analysis of our setup and results showed that the reason lies not in extensive variations or non-repeatable experiments, but has to do with the physical properties of MMS. Specifically, we believe that the inhomogeneities in the magnetic loading of the microspheres and the distribution of the magnetic component inside a nano- or microsphere has a large influence on the overall magnetophoretic behavior in a magnetic field which produces sub-saturation magnetization levels. Since the application of MMS for magnetic targeting inside patients normally involves magnetic fields similar to the ones used in our microscopic setup, our method might be important for simulating the in vivo behavior. Despite its shortcomings, our method seems to be a useful tool. However, our results should be further examined and confirmed in different setups, both in vitro and in vivo.

Acknowledgments

This work was made possible by an AFOSR/DARPA seedling grant and partial support for Martin Lobedann from the Bundesministerium für Bildung und Forschung (BMBF), InnoRegio BioMeT network, Germany, grant 03I4013A. We thank micromod GmbH (Rostock, Germany), chemicell GmbH (Berlin, Germany), FeRx Inc. (San Diego, CA, USA) and MO-SCI Corp. (Rolla, MO, USA) to provide us with MMS samples for this project. We are also thankful to Dr. Elke Boschke, who made this practical training possible for Martin Lobedann. We appreciate the many good ideas of Judy Drazba Ph.D. and Amit Vasanji in the imaging core at the Lerner Research Institute, Cleveland Clinic Foundation, to improve the microscopy and computer analysis. We also thank Dave Schumick for the schematic drawings

in Figs. 1 and 4, Dr. Daniel Duguay to provide us with a copy of his master's thesis, and Lydia Cartar for help in writing the manuscript.

References

[1] U.O. Häfeli, in: R. Arshady, K. Kono (Eds.), The MML Series, vol. 8, Citrus Books, London.
[2] U.O. Häfeli, Int. J. Pharm. 277 (2004) 19.
[3] W. Schütt, C. Grüttner, U. Häfeli, et al., Hybridoma 16 (1997) 109.
[4] R. Arshady, Microspheres, Microcapsules & Liposomes: Magneto- and Radiopharmaceuticals, vol. 3, first ed., Citus Books, London, 2001.
[5] S.J. Gill, C.P. Malone, M. Downing, Rev. Sci. Instrum. 31 (1960) 1299.
[6] L.F. Lindoy, V. Katovic, D.H. Busch, J. Chem. Educ. 49 (1972) 117.
[7] L. Petersson, A. Ehrenberg, Rev. Sci. Instrum. 56 (1985) 575.
[8] O. Beuf, A. Briguet, M. Lissac, et al., J. Magn. Reson. Ser. B 112 (1996) 111.
[9] C.B. Fuh, S.Y. Chen, J. Chromatogr. A 857 (1999) 193.
[10] Y. Jiang, M.E. Miller, M.E. Hansen, et al., J. Magn. Magn. Mater. 194 (1999) 53.
[11] S. Reddy, L.R. Moore, L. Sun, et al., Chem. Eng. Sci. 51 (1996) 947.
[12] L.R. Moore, M. Zborowski, M. Nakamura, et al., J. Biochem. Biophys. Methods 44 (2000) 115.
[13] S. Winoto-Morbach, W. Müller-Ruchholtz, Eur. J. Pharm. Biopharm. 41 (1995) 55.
[14] H. Watarai, M. Suwa, Y. Iiguni, Anal. Bioanal. Chem. 378 (2004) 1693.
[15] T. Abbasov, S. Herdem, M. Köksal, J. Phys. D: Appl. Phys. 32 (1999) 1097.
[16] U.O. Häfeli, R. Ciocan, J.P. Dailey, Eur. Cells Mater. 3 (Suppl. 2) (2002) 24.
[17] N. Nakamura, M. Zborowski, L.C. Lasky, et al., Exp. Fluids 30 (2001) 371.
[18] M. Zborowski, G. Ostera, L.R. Moore, et al., Biophys. J. 84 (2003) 2638.
[19] R.C. Weast, CRC Handbook of Chemistry and Physics, 62nd ed., CRC Press, Boca Raton, FL, 1981.
[20] D.G. Duguay, Master's Thesis, McGill, Montreal, Canada, 1991.
[21] U.O. Häfeli, S.M. Sweeney, B.A. Beresford, et al., Nucl. Med. Biol. Int. J. Rad. Appl. Instr. Part B 22 (1995) 147.